RESEARCH ARTICLE | DECEMBER 19 2023

Conformal invariance of 2D quantum turbulence in an exciton–polariton fluid of light

R. Panico ; A. S. Lanotte ; D. Trypogeorgos ; G. Gigli ; M. De Giorgi ; D. Sanvitto ; D. Ballarini

Appl. Phys. Rev. 10, 041418 (2023)
https://doi.org/10.1063/5.0167655

Applied Physics Reviews ARTICLE pubs.aip.org/aip/are

Conformal invariance of 2D quantum turbulence in an exciton–polariton fluid of light

Cite as: Appl. Phys. Rev. **10**, 041418 (2023); doi: 10.1063/5.0167655
Submitted: 14 July 2023 · Accepted: 27 November 2023 ·
Published Online: 19 December 2023

R. Panico,[1] A. S. Lanotte,[1,2] D. Trypogeorgos,[1] G. Gigli,[1,3] M. De Giorgi,[1] D. Sanvitto,[1] and D. Ballarini[1,a)]

AFFILIATIONS

[1]CNR NANOTEC, Institute of Nanotechnology, Via Monteroni, 73100 Lecce, Italy
[2]INFN, Sez. Lecce, 73100 Lecce, Italy
[3]Dipartimento di Matematica e Fisica E. De Giorgi, Università del Salento, Campus Ecotekne, via Monteroni, Lecce 73100, Italy

[a)]Author to whom correspondence should be addressed: dario.ballarini@nanotec.cnr.it

ABSTRACT

The similarities of quantum turbulence with classical hydrodynamics allow quantum fluids to provide essential models of their classical analog, paving the way for fundamental advances in physics and technology. Recently, experiments on 2D quantum turbulence observed the clustering of same-sign vortices in strong analogy with the inverse energy cascade of classical fluids. However, self-similarity of the turbulent flow, a fundamental concept in the study of classical turbulence, has so far remained largely unexplored in quantum systems. Here, thanks to the unique features of exciton–polaritons, we measure the scale invariance of velocity circulations and show that the cascade process follows the universal scaling of critical phenomena in 2D. We demonstrate this behavior from the statistical analysis of the experimentally measured incompressible velocity field and the microscopic imaging of the quantum fluid. These results can find wide application in both quantum and classical 2D turbulence.

I. INTRODUCTION

Turbulent dynamics in classical fluids has been first identified by A. N. Kolmogorov with the presence of a self-similar energy cascade. Self-similarity, or scale invariance, refers to the statistically identical behavior of the velocity fluctuations after scale transformations. In three dimensions (3D), the existence of non-zero energy dissipation even in the limit of zero viscosity implies a direct energy cascade from a large injection scale toward smaller spatial scales.[1] Turbulent energy cascades are the hallmark of far-from-equilibrium statistical behavior since energy injected in the system never attains equipartition. Instead, the non-linear energy transfer is irreversible, meaning that it has a preferred direction: when such transfer goes on average from large toward smaller eddies, it is defined as direct, and this is the case of kinetic energy in incompressible three-dimensional classical fluids. In two dimensions (2D), the picture is different due to the existence, in addition to kinetic energy, of another integral of motion given by enstrophy, i.e., the mean squared vorticity. Since kinetic energy and enstrophy cannot cascade in the same direction, a different scenario emerges: while enstrophy undergoes a direct cascade from the injection scale toward smaller scales, the kinetic energy does the opposite and flows on average from the scale of injection toward larger spatial structures, in a process called inverse energy cascade.[2,3]

A subtler consequence of the direction of the cascade concerns the presence of intermittency that is the deviation from self-similarity. Indeed, direct turbulent cascades are generally not scale invariant,[4] in connection with the non-Gaussian nature of the small scales viscous processes. This is the case for 3D turbulence, where most of the kinetic energy is dissipated within spatially localized structures. This intermittent statistics of energy dissipation breaks the original Kolmogorov assumption of self-similarity of the cascade process.[5,6] The 2D energy cascade in classical turbulence is fundamentally different: the presence of intermittency in the inverse transfer process has been ruled out,[3,7,8] intuitively because the energy fluxes are directed toward larger structures where extreme events due to energy dissipation play no role. Hence, general understanding suggests that velocity fluctuations are scale-invariant in the inverse energy cascade.

Quantum turbulence, differently from its classical counterpart, is intrinsically singular since its basic constituents are discrete, quantized vortices of unitary topological charge. Nevertheless, both quantum and classical turbulence exhibit energy cascades, and the observation of an inverse energy cascade in 2D quantum fluids has been a recent

development.[9–11] In 2D, quantum vortices resemble the point vortex model proposed by L. Onsager, who described the final stage of the inverse cascade as an equilibrium state in a negative temperature regime.[12,13] Starting from a Hamiltonian model of a 2D flow in terms of discrete vortices, Onsager suggested that at sufficiently high energy, equal sign vortices would approach each other in large cluster, beating their mutual repulsion, and that this result could explain the appearance of large spatial structures in two-dimensional flows.

The experimental investigation of quantum turbulence, which began with superfluid helium,[14,15] has made great progress with the realization of Bose–Einstein condensates (BEC) of ultracold atoms.[16–19] One of the main reasons why BECs are important for the study of quantum turbulence is the possibility of visualizing individual vortices and describing their dynamics on a microscopic level.[20] On the other hand, an open question is how to bridge the gap between the discrete picture of quantum vortices and the self-similar nature of classical inverse energy cascade.[21] In particular, we wonder whether the self-similar spatial correlations may nonetheless emerge in the velocity field of a quantum fluid, and which are the roots of this evidence in the system dynamics.

For this purpose, we use an optical system, exciton–polaritons in semiconductor microcavities. These hybrid light–matter quasiparticles have been shown in the last few decades to behave like a quantum fluid of light, manifesting out-of-equilibrium Bose–Einstein condensation and superfluidity.[22–25] We have recently shown that, under suitable initial conditions, it is possible to induce an inverse cascade of incompressible kinetic energy in 2D polariton quantum fluids.[11] Crucially, these systems allow the measurement of the spatial distribution of the velocity field with high accuracy, enabling a robust statistical analysis.[26,27]

Here, thanks to the direct measurement of the phase of the polariton field, we are able to extract the statistics of the incompressible velocity in the inverse energy cascade of a quantum fluid. While the singular nature of quantized vortices manifests itself in the large tails of velocity increment distribution, the velocity circulations (or vorticity fluxes) show remarkable scale invariant properties. Moreover, we find that a coarse graining of the vorticity field allows the identification of macro-regions of aligned vortex–antivortex dipoles that are responsible for the appearance of long-range order in the system. We show that the statistical distribution and fractal dimension of the regions with correlated vorticity follow the critical behavior predicted near phase transition in percolation theory. This analysis goes beyond the classification of first-neighbor vortices and opens to the investigation of spatial symmetries in 2D quantum turbulence.

II. MAIN RESULTS

We use the same experimental configuration described in a previous work[11] to induce vortex clustering and a transient regime of inverse kinetic energy cascade after the expansion of a polariton quantum fluid in a confining potential (see supplementary material). The typical number of vortices is $N > 80$, with intervortex distances $\approx 2\xi$ and diameter of the confining ring potential $> 50\xi$, being $\xi = 2.3\ \mu$m the estimated healing length of the quantum fluid. For our analysis, we consider the incompressible velocity field $\mathbf{u}(\mathbf{x}, t)$ of the 2D polariton fluid described by the wave-function $\psi(\mathbf{x}, t) = \sqrt{\rho(\mathbf{x}, t)}e^{-i\theta(\mathbf{x},t)}$, in the time interval corresponding to the inverse energy cascade. The total velocity field is given by the gradient of the phase θ as

$$\mathbf{v}(\mathbf{x}, t) = \frac{\hbar}{m}\nabla\theta(\mathbf{x}, t), \tag{1}$$

where m is the polariton mass. The phase of the polariton fluid is obtained from time-resolved interferometric measurements of the photons emitted by the microcavity, while the incompressible component $\mathbf{u}(\mathbf{x}, t)$ of the velocity field is determined at any point in space by applying the Helmholtz decomposition to the density weighted velocity $\sqrt{\rho}\mathbf{v}$.[11] We use about 125K pixels per image with a spatial resolution $s \sim 0.14\xi$. In our experiments, each image is obtained by averaging thousands of pulses (see supplementary material). Vortex tracking remains viable due to the shallow potential landscape of our high-quality sample, which establishes favored positions for vortex nucleation and trajectories without pinning to spatial defects.[11,28] To improve statistical accuracy, we average over larger time intervals (always within the inverse energy cascade window), and over few realizations of the experiment in different locations of the sample. In the following, we show the statistics over a total number of pixels $\approx 2 \times 10^7$ (accounting for the longitudinal increments along both x and y axes).

In Fig. 1, the probability density function (PDF) of the longitudinal velocity increments $\delta_r u \equiv \frac{\mathbf{r}}{r} \cdot [\mathbf{u}(\mathbf{x} + \mathbf{r}) - \mathbf{u}(\mathbf{x})]$, where the velocity $\mathbf{u}$ and the separation $\mathbf{r}$ vectors are taken in the same direction, are shown for increasing spatial scale $r = |\mathbf{r}|$, from $r \simeq 0.4\xi$ to $r \simeq 14\xi$. At very small scales, the velocity increment PDF follows a Cauchy distribution, while it gradually approaches a Gaussian distribution as the scale increases.[29] The presence of exponential tails in the distribution is clearly visible for every distance, indicating a finite probability of large $|\delta_r u|$ events. This follows directly from the presence of quantized vortices, where velocity increments manifest their singular behavior.[29] This reflects as well in the lack of self-similarity of the PDFs when rescaled to their standard deviations as in Fig. 1—self-similarity would entail a

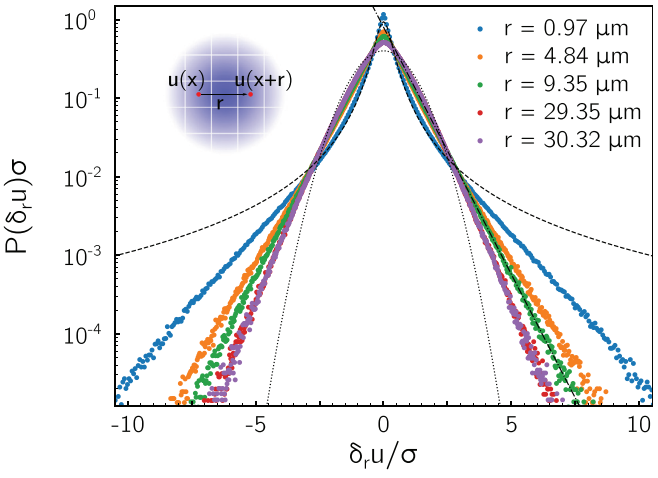

FIG. 1. Probability density functions (PDF) of the longitudinal velocity increments $\delta_r u \equiv \frac{\mathbf{r}}{r} \cdot [\mathbf{u}(\mathbf{x} + \mathbf{r}) - \mathbf{u}(\mathbf{x})]$ at scale $\mathbf{r}$, normalized to their standard deviation $\sigma = \langle(\delta_r u)^2\rangle^{1/2}$. For sub-healing length scales, $r < \xi = 2.3\ \mu$m, the PDF follows a Cauchy–Lorentz distribution (dashed line), while at increasing $\mathbf{r}$ it slowly approaches a Gaussian (dotted line). For every scale, the tails of the distribution are exponential (dashed-dotted line). Note that the mean inter-vortex distance corresponds to $\sim 5\ \mu$m. The lack of a self-similar rescaling of the PDFs is the manifestation of the singular nature of the vortices and an indication of intermittency.

collapse of the PDFs onto a single curve, as observed in the classical case.[8] Deviations from Gaussianity, which have been reported for velocity distributions in 3D as well as in 2D,[30,31] can be related to the fact that energy is injected spontaneously through the nucleation of vortex dipoles at the healing length scale.[32]

While the distribution of the velocity increments is not a good observable to look for scale-invariant properties in a quantum fluid, moments of velocity circulation have recently been proposed as more fundamental and unifying quantities.[33–35] Velocity circulation is defined as

$$\Gamma_R(\mathbf{x}) = \oint_{C_R} \mathbf{u}(\mathbf{x}') \cdot d\mathbf{x}', \tag{2}$$

where C_R is a square loop with opposite corners $(x - R/2, y - R/2)$ and $(x + R/2, y + R/2)$, while $\mathbf{u}$ is the incompressible velocity. In Fig. 2, we show the PDFs of the velocity circulation, measured on closed loops of size R. The most striking feature is that scale invariance now holds: contrary to the case of velocity increments, the PDF of the velocity circulation on loops of different size rescale with their standard deviation and collapse on a single (exponential) distribution. Incidentally, we remark that at difference with the locality regime of classical inverse cascade, the scaling behaviors of velocity and vorticity cannot be directly linked in a quantum system.

Self-similarity is a strong feature that suggests the quest for other global symmetries. Numerical results on classical 2D turbulence have shown that lines of zero-vorticity, i.e., the boundaries of high vorticity regions, are stochastic Schramm–Loewner evolution (SLE_κ) curves.[36] The SLE curves univocally describe the conformal invariant scaling limit of the interfaces of many 2D critical models, with the parameter κ defining the universal behavior close to threshold. The same universality class was predicted for cluster boundaries of critical percolation, one of the most fundamental models of phase transition, and the isovorticity lines in the inverse energy cascade, also for weakly compressible fluids.[37]

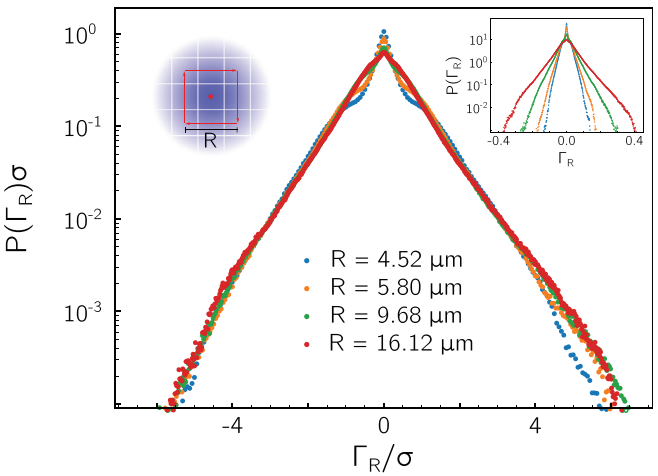

FIG. 2. PDF of the vorticity across the surface S_R enclosed in the loop of size R, defined as in Eq. (3), normalized to its standard deviation $\sigma \equiv \langle \Gamma_R^2 \rangle^{1/2}$. The PDFs for different values of R all rescale to the same exponential distribution, showing how the velocity circulation is scale invariant. For comparison, the inset shows the PDF for the velocity circulations Γ_R with the same values of R but without rescaling.

To explore the appearance of conformal invariant interfaces in 2D quantum turbulence, we consider a continuous field of coarse-grained vorticity $\boldsymbol{\omega} = \nabla \times \mathbf{u}$ (i.e., its flux), defined at each point in space as the value of velocity circulation $\Gamma_R(\mathbf{x})$ over a square loop of size comparable to the healing length ξ. Via the Stokes' theorem, we calculate for each point $\mathbf{x} = (x, y)$ the vorticity flux through the surface S_R enclosed in the loop C_R as

$$\Gamma_R(\mathbf{x}) = \int_{S_R} \left(\nabla \times \mathbf{u}(\mathbf{x}')\right) \cdot d\mathbf{S}_R(\mathbf{x}'). \tag{3}$$

The scalar field $\Gamma_R(\mathbf{x})$ combines the information about the sign and distribution of dipoles, smoothing the singularities of quantum vortices. The 2D maps of $\Gamma_R(\mathbf{x})$ are binarized using an upper (lower)

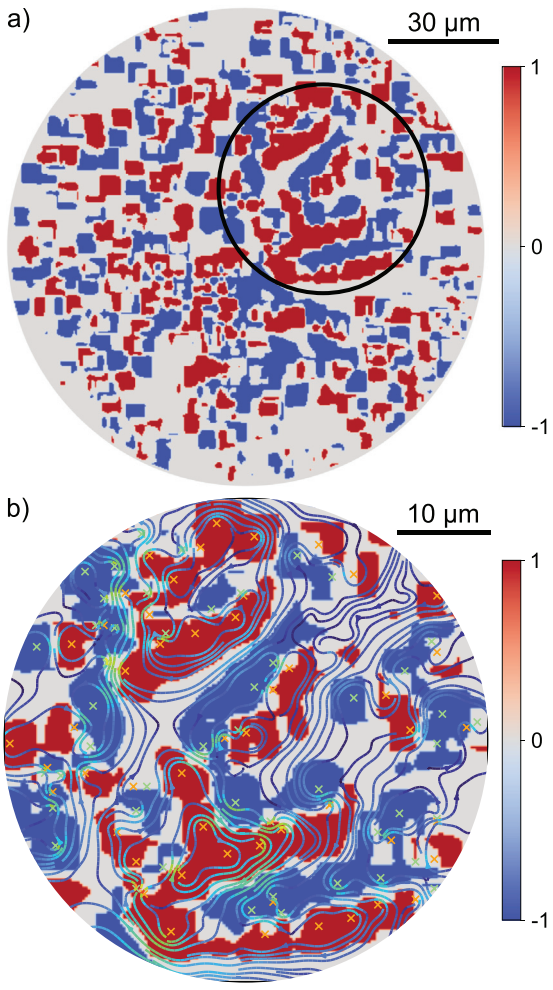

FIG. 3. (a) Circulation map of a single frame obtained using Eq. (3) with $R \simeq 2\xi$, showing the connected areas with a circulation value above 10% of its maximum. (b) Zoom of the spatial region [black circle in (a)], to better contrast areas of isovorticity flux with respect to the velocity field streamlines; the positions of the vortices (orange) and antivortices (green) are also reported. The overlap between closed velocity lines and the areas we identified is considerable and directly related to specific orientation of the dipoles.

threshold to identify the areas with correlated vorticity (see methods). In Fig. 3(a), we show a typical 2D map for $\Gamma_{2\xi}(\mathbf{x})$ with a threshold of 10% of its maximum value. In Fig. 3(b), the region within the black circle in Fig. 3(a) is magnified to show the underlying organization of vortices and velocity streamlines. The regions with same sign of $\Gamma_{2\xi}(\mathbf{x})$ are indicated in red and blue, for positive and negative fluxes, respectively. Vortices and antivortices are also indicated in Fig. 3(b), showing the close relation between dipole orientation and the formation of extended regions with similar vorticity. While a first neighbor classification would only count the presence of a large number of dipoles, here, we identify clusters of aligned vortex dipoles forming coherent structures that extend over several healing lengths.

We focus on the statistics of the vorticity (flux) clusters and on that of their boundaries, for which percolation theory predictions have already been tested in classical turbulence.[36,37] In Fig. 4(a), we show the distribution $n(A)$ of regions with area A, identified as in Fig. 3(b). The PDF decreases as a power law $n(A) \propto A^{-\alpha}$, with the same exponent α independently from the threshold used. The dashed black line scales as $\propto A^{-96/91-1}$ and characterizes the cluster size distribution at the percolation threshold,[38] showing good agreement with the experimental results above the healing length. In the absence of the energy cascade, we do not observe such clear scaling of the size distribution, as shown in the supplementary material.

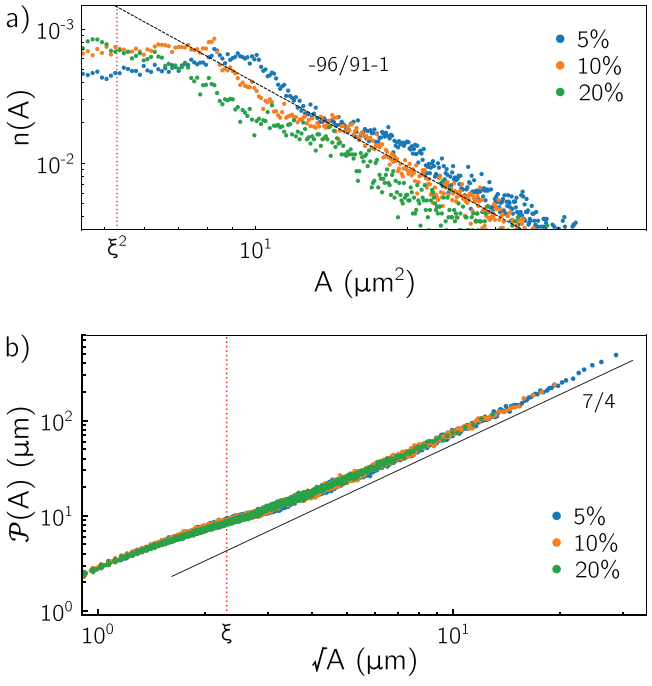

FIG. 4. (a) Distribution of the extension of the connected areas of iso-vorticity flux, calculated on the binarized maps of Γ_R taking into account different thresholds with respect to the maximum value (5%, 10%, 20%). The distribution scales with the exponent $\alpha \simeq 96/91 + 1 \simeq 2.05$ for values of the area above ξ^2, a value expected at the percolation threshold. (b) Fractal dimension of the connected regions [same as in (a)] computed as the perimeter of each region vs their size, i.e., the square root of their area, yielding a value of $D = 7/4$, which corresponds to the SLE prediction for percolation.

One of the central predictions for SLE curves is their fractal dimension, which is known to be $D = 1 + \kappa/8$ and, for percolation, $\kappa = 6$ and $D = 7/4$. In Fig. 4(b), we plot the perimeter $\mathcal{P}(A)$ vs the square root of the intrinsic area A of the connected regions. A clear scaling $\mathcal{P}(A) \propto (\sqrt{A})^D$ appears, with the exponent D, indicating the fractal dimension, which is $D > 1$. The black line in Fig. 4(b) is the SLE prediction for percolation, $D = 7/4$, which shows a good agreement with the experimental results above the healing length. In the absence of the inverse energy cascade, the perimeter-area scaling is limited by the smaller spatial extension of the isovorticity regions (see supplementary material), which have maximum size of $\approx 2.5\xi$ as compared to more than 10ξ in Fig. 4(b).

III. CONCLUSIONS

To our knowledge, this is the first experimental measurement of the statistics of the velocity field in turbulent 2D quantum fluids. Our experiments show that the scale invariance of classical turbulence can be retrieved by considering velocity circulation instead of velocity increments.[33,34] By the coarse graining of the vorticity field, isovorticity regions are probed at scales larger than the intervortex distance, averaging out the singularities associated with the vortex cores.[31] Based on the scale-invariance of the circulations, we establish a connection with critical models in 2D. Real space analysis allows the identification of correlated vorticity regions with typical size ranging from ξ to 10ξ. We find that these regions share the same statistical behavior of critical percolation boundaries, enabling a series of predictions to be made on the properties of the inverse energy cascade in 2D quantum fluids. Optical systems provide a new experimental platform that can help unifying the microscopic nature of vortex interactions with the macroscopic symmetries of turbulent flows.[39–50]

SUPPLEMENTARY MATERIAL

See the supplementary material for a description and sketch of the experimental setup and information about the semiconductor microcavity sample, a discussion and data of the second order moment of longitudinal velocity increments, and a comparison with non-turbulent regime.

ACKNOWLEDGMENTS

The authors thank Guido Boffetta and Giorgio Krstulovic for useful discussions. The authors acknowledge the following projects: Italian Ministry of University (MUR) PRIN project "Interacting Photons in Polariton Circuits"—INPhoPOL (Grant No. 2017P9FJBS); the project "Hardware implementation of a polariton neural network for neuromorphic computing"—Joint Bilateral Agreement CNR-RFBR (Russian Foundation for Basic Research)—Triennal Program 2021–2023; the MAECI project "Novel photonic platform for neuromorphic computing," Joint Bilateral Project Italia-Polonia 2022–2023; PNRR MUR project "National Quantum Science and Technology Institute"—NQSTI (PE0000023); PNRR MUR project "Integrated Infrastructure Initiative in Photonic and Quantum Sciences"—I-PHOQS (IR0000016); Apulia Region, project "Progetto Tecnopolo per la Medicina di precisione," Tecnomed 2 (Grant No. Deliberazione della Giunta Regionale n. 2117 del 21/11/2018). This work was also funded by the European Union, HORIZON-EIC-2022-PATHFINDER CHALLENGES project Q-ONE (Grant

101115575). The authors are grateful to P. Cazzato for the valuable technical support during the experiments.

AUTHOR DECLARATIONS

Conflict of Interest

The authors have no conflicts to disclose.

Author Contributions

Riccardo Panico: Conceptualization (equal); Data curation (equal); Investigation (lead); Software (lead); Supervision (lead); Writing – original draft (equal); Writing – review & editing (equal). **Alessandra Sabina Lanotte:** Data curation (equal); Formal analysis (equal); Investigation (equal); Software (lead); Writing – review & editing (equal). **Dimitrios Trypogeorgos:** Formal analysis (equal); Investigation (supporting); Writing – review & editing (equal). **Giuseppe Gigli:** Funding acquisition (equal); Investigation (supporting); Resources (equal). **Milena De Giorgi:** Investigation (supporting); Project administration (equal). **Daniele Sanvitto:** Investigation (equal); Resources (equal); Writing – review & editing (equal). **Dario Ballarini:** Conceptualization (equal); Funding acquisition (equal); Investigation (equal); Resources (equal); Supervision (lead); Writing – original draft (equal); Writing – review & editing (equal).

DATA AVAILABILITY

The data that support the findings of this study are available from the corresponding author upon reasonable request.

APPENDIX: METHODS

To build a statistics for the connected regions of vorticity flux like the one shown in Fig. 3, we first compute the curl of the incompressible velocity field $\nabla \times \mathbf{u}(\mathbf{x})$ and then we construct the scalar field $\Gamma_R(\mathbf{x})$, for each image and for $R = [1.4\xi,\ 1.96\xi,\ 2.5\xi]$. The highest positive (minimum negative) value for this ensemble of fields $\Gamma_R(\mathbf{x})$ is what we use to set a threshold that is 5%, 10%, or 20% of this value. For each field every positive (negative) value that is greater (smaller) than said threshold is set to 1 (-1), while the rest is set to 0, resulting in the "binarized" images like the one in Fig. 3(a).

To analyze the resulting connected regions, we labeled them with the python *skimage.measure.label* module, using a 2-connectivity. The area of each region is the number of pixels of the region scaled by the pixel area, while the perimeter is approximated with a line through the centers of border pixels using a 4-connectivity.

REFERENCES

[1]U. Frisch, *Turbulence: The Legacy of A. N. Kolmogorov* (Cambridge University Press, 1995).
[2]R. H. Kraichnan, Phys. Fluids **10**, 1417 (1967).
[3]G. Boffetta and R. E. Ecke, Annu. Rev. Fluid Mech. **44**, 427 (2012).
[4]A. Alexakis and L. Biferale, Phys. Rep. **767–769**, 1–101 (2018).
[5]P. K. Yeung, X. M. Zhai, and K. R. Sreenivasan, Proc. Natl. Acad. Sci. U. S. A. **112**, 12633 (2015).
[6]R. Benzi, G. Paladin, G. Parisi, and A. Vulpiani, J. Phys. A **17**, 3521 (1984).
[7]J. Paret and P. Tabeling, Phys. Fluids **10**, 3126–3136 (1998).
[8]G. Boffetta, A. Celani, and M. Vergassola, Phys. Rev. E **61**, R29 (2000).
[9]S. P. Johnstone, A. J. Groszek, P. T. Starkey, C. J. Billington, T. P. Simula, and K. Helmerson, Science **364**, 1267 (2019).
[10]G. Gauthier, M. T. Reeves, X. Yu, A. S. Bradley, M. A. Baker, T. A. Bell, H. Rubinsztein-Dunlop, M. J. Davis, and T. W. Neely, Science **364**, 1264 (2019).
[11]R. Panico, P. Comaron, M. Matuszewski, A. S. Lanotte, D. Trypogeorgos, G. Gigli, M. D. Giorgi, V. Ardizzone, D. Sanvitto, and D. Ballarini, Nat. Photonics **17**, 451 (2023).
[12]L. Onsager, Il Nuovo Cimento (1943-1954) **6**, 279 (1949).
[13]G. L. Eyink and K. R. Sreenivasan, Rev. Mod. Phys. **78**, 87 (2006).
[14]H. E. Hall, W. F. Vinen, and D. Shoenberg, "The rotation of liquid helium II II. The theory of mutual friction in uniformly rotating helium II," Proc. R. Soc. London, Ser. A **238**, 215 (1956).
[15]C. F. Barenghi, L. Skrbek, and K. R. Sreenivasan, Proc. Natl. Acad. Sci. **111**, 4647 (2014).
[16]E. A. L. Henn, J. A. Seman, G. Roati, K. M. F. Magalhães, and V. S. Bagnato, Phys. Rev. Lett. **103**, 045301 (2009).
[17]A. C. White, B. P. Anderson, and V. S. Bagnato, Proc. Natl. Acad. Sci. **111**, 4719 (2014).
[18]N. Navon, A. L. Gaunt, R. P. Smith, and Z. Hadzibabic, Nature **539**, 72 (2016).
[19]N. Navon, R. P. Smith, and Z. Hadzibabic, Nat. Phys. **17**, 1334 (2021).
[20]W. J. Kwon, G. Del Pace, K. Xhani, L. Galantucci, A. Muzi Falconi, M. Inguscio, F. Scazza, and G. Roati, Nature **600**, 64 (2021).
[21]A. Skaugen and L. Angheluta, Phys. Rev. E **95**, 052144 (2017).
[22]I. Carusotto and C. Ciuti, Rev. Mod. Phys. **85**, 299 (2013).
[23]A. Amo, D. Sanvitto, F. Laussy, D. Ballarini, E. del Valle, M. Martin, A. Lemaitre, J. Bloch, D. Krizhanovskii, M. Skolnick *et al.*, Nature **457**, 291 (2009).
[24]D. Caputo, D. Ballarini, G. Dagvadorj, C. Sánchez-Muñoz, M. DeGiorgi, L. Dominici, K. West, L. N. Pfeiffer, G. Gigli, F. P. Laussy, M. H. Szymańska, and D. Sanvitto, Nat. Mater. **17**, 145 (2018).
[25]D. Ballarini, D. Caputo, G. Dagvadorj, R. Juggins, M. D. Giorgi, L. Dominici, K. West, L. N. Pfeiffer, G. Gigli, M. H. Szymańska *et al.*, Nat. Commun. **11**, 217 (2020).
[26]S. Donati, L. Dominici, G. Dagvadorj, D. Ballarini, M. De Giorgi, A. Bramati, G. Gigli, Y. G. Rubo, M. H. Szymańska, and D. Sanvitto, Proc. Natl. Acad. Sci. **113**, 14926 (2016).
[27]R. Panico, G. Macorini, L. Dominici, A. Gianfrate, A. Fieramosca, M. De Giorgi, G. Gigli, D. Sanvitto, A. S. Lanotte, and D. Ballarini, Phys. Rev. Lett. **127**, 047401 (2021).
[28]K. G. Lagoudakis, F. Manni, B. Pietka, M. Wouters, T. C. H. Liew, V. Savona, A. V. Kavokin, R. André, and B. Deveaud-Plédran, Phys. Rev. Lett. **106**, 115301 (2011).
[29]I. Min, I. Mezić, and A. Leonard, Phys. Fluids **8**, 1169 (1996).
[30]A. White, C. F. Barenghi, N. A. Proukakis, A. J. Youd, and D. H. Wacks, Phys. Rev. Lett. **104**, 075301 (2010).
[31]A. W. Baggaley and C. F. Barenghi, Phys. Rev. E **84**, 067301 (2011).
[32]G. Sofiadis, I. E. Sarris, and A. Alexakis, Phys. Rev. Fluids **8**, 024607 (2023).
[33]K. P. Iyer, K. R. Sreenivasan, and P. K. Yeung, Phys. Rev. X **9**, 041006 (2019).
[34]J. I. Polanco, N. P. Mueller, and G. Krstulovic, Nat. Commun. **12**, 7090 (2021).
[35]H.-Y. Zhu, J.-H. Xie, K.-Q. Xia *et al.*, Phys. Rev. Lett. **130**, 214001 (2023).
[36]D. Bernard, G. Boffetta, A. Celani, and G. Falkovich, Nat. Phys. **2**, 124 (2006).
[37]L. Puggioni, A. G. Kritsuk, S. Musacchio, and G. Boffetta, Phys. Rev. E **102**, 023107 (2020).
[38]D. Stauffer and A. Aharony, *Introduction to Percolation Theory* (Taylor & Francis, 2003).
[39]D. Caputo, N. Bobrovska, D. Ballarini, M. Matuszewski, M. De Giorgi, L. Dominici, K. West, L. N. Pfeiffer, G. Gigli, and D. Sanvitto, Nat. Photonics **13**, 488 (2019).
[40]I. Liberal, M. Lobet, Y. Li, and N. Engheta, Proc. Natl. Acad. Sci. **117**, 24050 (2020).
[41]A. A. Maître, F. Claude, G. Lerario, S. Koniakhin, S. Pigeon, D. Solnyshkov, G. Malpuech, Q. Glorieux, E. Giacobino, and A. Bramati, Europhys. Lett. **134**, 24004 (2021).
[42]A. Eloy, O. Boughdad, M. Albert, P. Larré, L. Mortessagne, M. Bellec, and C. Michel, Europhys. Lett. **134**, 26001 (2021).
[43]T. Ferreira, V. Rocha, D. Silva, A. Guerreiro, and N. Silva, New J. Phys. **24**, 113050 (2022).
[44]H. Li, Z. Zhou, W. Sun, M. Lobet, N. Engheta, I. Liberal, and Y. Li, Nat. Commun. **13**, 4747 (2022).
[45]M. Abobaker, W. Liu, T. Aladjidi, A. Bramati, and Q. Glorieux, arXiv:2211.08441 (2023).

[46]L. H. Dogra, G. Martirosyan, T. A. Hilker, J. A. P. Glidden, J. Etrych, A. Cao, C. Eigen, R. P. Smith, and Z. Hadzibabic, Nature **620**, 521 (2023).
[47]A. D. Garcia-Orozco, L. Madeira, M. A. Moreno-Armijos, A. R. Fritsch, P. Tavares, P. Castilho, A. Cidrim, V. Roati, and G. Bagnato, Phys. Rev. A **106**, 023314 (2022).
[48]X. Bai, W. Wang, J. Zhang, Y. Wang, and Y. Xiang, arXiv:2305.11884v2 (2023).
[49]Y. Xiong, J. Chen, and X. Yu, Commun. Theor. Phys. **75**(9), 095101 (2023).
[50]T. Congy, P. Azam, R. Kaiser, and N. Pavloff, "Topological constraints on the dynamics of vortex formation in a bi-dimensional quantum fluid," arXiv:2308.02305 (2023).